Available online at www.sciencedirect.com
SCIENCE DIRECT®
Journal of Power Sources 144 (2005) 113–121
JOURNAL OF POWER SOURCES
www.elsevier.com/locate/jpowsour

Adhesive copper films for an air-breathing polymer electrolyte fuel cell

F. Jaouen [a,*], S. Haasl [b], W. van der Wijngaart [b], A. Lundblad [a], G. Lindbergh [a], G. Stemme [b]

[a] *Department of Chemical Engineering and Technology, Applied Electrochemistry, The Royal Institute of Technology (KTH), Teknikringen 42, SE-100 44 Stockholm, Sweden*

[b] *Department of Signals, Sensors and Systems, Microsystems Technology, The Royal Institute of Technology (KTH), SE-100 44 Stockholm, Sweden*

Received 18 October 2004; received in revised form 20 December 2004; accepted 20 December 2004
Available online 19 February 2005

Abstract

A design for an air-breathing and passive polymer electrolyte fuel cell is presented. Such a type of fuel cell is in general promising for portable electronics. In the present design, the anode current collector is made of a thin copper foil. The foil is provided with an adhesive and conductive coating, which firstly tightens the hydrogen compartment without mask or clamping pressure, and secondly secures a good electronic contact between the anode backing and the current collector. The cathode comprises a backing, a gold-plated stainless steel mesh and a current collector cut out from a printed circuit board. Three geometries for the cathode current collector were evaluated. Single cells with an active area of 2 cm^2 yielded a peak power of 250–300 $mW\,cm^{-2}$ with air and pure H_2 in a complete passive mode except for the controlled flow of H_2. The cells' response was investigated in steady state and transient modes.

Keywords: Polymer; Fuel cell; Breathing; Adhesive; Copper

1. Introduction

Unlike the situation for stationary or transportation applications (1–200 kW), the main motivation for developing small polymer electrolyte fuel cells (micro to hundreds of watts) does not reside in environmental benefits but in foreseeable improved technical characteristics compared to the established technologies, which are chiefly primary and secondary batteries. Also, material costs are a lesser barrier than in transportation applications since batteries are relatively expensive [1]. The end-user price for a laptop battery pack rated to 45–60 Wh lies at US$ 100–250. Assuming the battery packs are designed to give an average output of 40 W, this gives a cost of US$ 2500–6000 kW^{-1}. These figures are about two decades larger than the target for material costs for polymer fuel cells in car engines (US$ 50 kW^{-1}). The expected advantages of Polymer Electrolyte Fuel Cells (PEFCs) (acronym not constrained to any particular fuel) against batteries are a higher energy density (Wh g^{-1}) and no recharging time. Their plots of system volume or weight against energy content (Wh) can be described as two lines crossing each other, the gentler line characterizing PEFCs [1]. This means that above a threshold power, PEFCs become more attractive than batteries. Today's most efficient lithium batteries reach a weight power density of 130 Wh kg^{-1} (charger excluded), while it has been calculated by Kelley et al. [2] that a direct methanol fuel cell with a molar ratio of 1:10 in methanol:water could yield 300 Wh kg^{-1}, and with a 1:1 molar ratio roughly 1000 Wh kg^{-1}. Also, a niche market could pop up for primary fuel cells with encapsulated fuel not destined to be replace. Such cells could be made of non-noble catalysts and non-fluorinated polymers and address applications with reduced lifetime. Yet, the electrical needs of wireless applications are very scattered. The duty cycle, average and peak power requirements of each specific application

* Corresponding author. Present address: INRS-EMT, 1650 Bd Lionel-Boulet, Varennes, Que., Canada J3X 1S2. Tel.: +1 514 929 8143; fax: +1 514 929 8102.
E-mail addresses: jaouen@inrs-emt.uquebec.ca (F. Jaouen), sjoerd@s3.kth.se (S. Haasl), wouter@s3.kth.se (W.v.d. Wijngaart), anders.lundblad@ket.kth.se (A. Lundblad), goeran.lindbergh@ket.kth.se (G. Lindbergh), stemme@s3.kth.se (G. Stemme).

0378-7753/$ – see front matter © 2005 Elsevier B.V. All rights reserved.
doi:10.1016/j.jpowsour.2004.12.048

(sensor, pacemaker, laptop computer, mobile phone, etc.) will determine the most appropriate technology.

Hitherto, PEFC reactors have been developed chiefly for large cells, where the benefits of having certain regulations (temperature, reactant flows and humidity) were not outweighed by the implied weight and electrical consumption of the associated ancillary components (cooling system, compressors and fans, humidifiers). Typically, these components cannot be efficiently scaled down. Thus, a peculiarity of small fuel cells is that they must be designed to work with minimized control. The design has naturally shifted from stacks to planar cells; the latter offering enhanced heat removal and air access to the cathode. Any planar configuration implies in turn a mixed conductor/insulator pattern for serial connections. There are two ways to make a serial connection between in-plane cells. The first consists of having cathodes on either side and anodes on the other and every cathode being connected with the anode of the next cell. This is referred to as the banded design [3–5]. The connection is made either by creating breaches in the central area of the membrane or by leading the current aside the active area beyond the membrane edge and making the connection there. The latter choice avoids cutting out through the membrane and in so doing avoids the fastidious tightening of each anode separately. The second possibility of making a serial connection of in-plane cells is to construct the two cell-house plates with each having cathodes and anodes alternated along its surface. This is referred to as the flip-flop design [5]. It is then straightforward to electrically connect a cathode of one cell to the anode of the next one because they lie abreast. Unfortunately, there is a covert drawback in doing this. If the proton conducting membrane is uninterrupted from cell to cell, then such a connection is equivalent to a short circuit (also referred to as cross-talking) [5]. The short circuit cannot be completely avoided unless a membrane piece is cut for every cell. Regardless of the design chosen for the in-plane serial connection, passive PEFCs do request membranes showing small resistance and this even if the water only originates from the fuel cell reaction. This fact calls for thin membranes as long as fuel crossover is not a concern. With hydrogen, the crossover current density through Nafion 112 was measured to be about 3 mA cm^{-2} at a pressure of 2.2 bar [6]. Thus, if the PEFC works on average at current densities of 200 mA cm^{-2} or more, fuel crossover is not a concern and the thinness of the membrane is limited by its mechanical integrity. Thus, a passive PEFC with a thin membrane preferably will have little or no compression between its lower and upper plates. Hence, the various cell components must have small interfacial resistances upon low compression. Low compression also has the advantage of leaving the gas backings with a high porosity, which is favorable for air diffusion to the cathode. One sees that any planar design sets material's requirements that are different from those of a stack design. So far, three types of materials and their associated technologies have been investigated for small PEFCs.

(i) Miniaturization of conventional PEFC design with graphite or stainless steel plates for the current collectors (CC) and cell housing;
(ii) Silicon technology, either patterning of conductive/non-conductive path on silicon wafers [5,7,8] or development of methods to create in the wafer a complex architecture of porous silicon layers on top of channels for the reactant gases [9–11];
(iii) Printed Circuit Board (PCB) technology, use of a thin layer of copper on electrically insulating composite materials [12–14].

The ideas and achievements for the two last technologies are now briefly reviewed.

(i) Techniques based on silicon technology have been developed toward microfabrication of fuel cells on silicon wafers. It often comprises the electrochemical etching of silicon to form a porous layer followed by electropolishing of the wafer underneath to form the gas channels. The porous layer is then partly filled with platinum by, e.g. sputtering. Peak performances of 60 and 200 mW cm^{-2} were reached with forced flows of pure hydrogen and oxygen [8,10].
(ii) Recently, two teams reported the use of Printed Circuit Board technology for small PEFCs [12–14]. Peak performances of 100 and 200 mW cm^{-2} were reached with hydrogen and breathing [12] or forced flow of air [13], respectively, on single cells of 2–10 cm^2. Stable performance for up to 1500 h was demonstrated when copper was appropriately plated [14]. Amidst the claimed advantages of the PCB technology, the most crucial ones are mature technology, lightweight and stiff composite materials, and design flexibility comprising complex conductor/insulator patterns, either as a mono- or multi-layer design [13].

In this paper, a proof-of concept for an air-breathing PEFC is presented. The cell design is inspired from the use of the PCB technology previously mentioned. The main novelties of the present design are firstly an anode current collector made of an adhesive copper foil and secondly a three-layer cathode comprising a backing, a stainless steel mesh and a PCB with aperture(s) for air access.

2. Cell design and experimental

Five single cells were studied and they are labeled A1, A2, A3, B2 and C2. The letter stands for the geometry of the cathode current collector: 'A' for a strip with four holes for air, 'B' for a square with a single hole and 'C' for a square with an array of holes (Fig. 1A). The cathode CCs were cut out from a plain Printed Circuit Board. The PCB was a commercial epoxy-glass composite uniformly plated with a 30 μm thick copper layer on one side. The numbers 2 and 3 in the cell acronym mean that second and third cells were constructed.

Thus, cells A2 and A3 are replicates of cell A1. The Membrane Electrode Assemblies (MEAs) were Primea 5510 from Gore (0.3 mg Pt cm^{-2}, 25 μm thick membrane). Gas backings were Carbel products from Gore, with their hydrophobic side turned against the MEA. The anode CC was made of a copper foil having an electron-conductive adhesive film on one or on both sides. The suppliers were TESA and 3 M, respectively. The adhesive was based on a silver-filled acrylic substance. The thickness of the adhesive film and copper foil was about 5 and 70 μm, respectively. The anode current collector was supported by the cell house, a 5 mm-thick Plexiglas sheet, wherein gas channels were milled. The arrangement of these different elements to form the single cell is now described (Fig. 1). The Plexiglas item was cut and T-shaped channels were milled on the top side to later conduct hydrogen. A double-sided adhesive tape (but non-conductive) from 3 M was then stuck onto the Plexiglas, completely covering its upside surface and closing thereby the originally opened channels (tape not shown in Fig. 1). The protective layer on the upside of the adhesive tape was then peeled off, whereupon the copper foil was adhered, forming the anode current collector. Next, inlet and outlet for hydrogen to from the anode backing were formed by cutting out from the two-layer sandwich (adhesive copper foil/adhesive tape), the part that covered the facing segments of the T-shaped channels. Then, after removal of the upside protective layer of the copper foil, a piece of Carbel backing of dimensions 14 mm × 14 mm (about 2 cm^2) was centered so as to cover the gas inlet and outlet and gently stuck onto the anode copper foil. The dimensions of this backing determined the active area of the cell. Then, a piece of MEA with dimensions 25 mm × 25 mm was cut out, and centered over the anode backing. The surface of the MEA not covering the backing was then sealed against the anode copper foil by softly wiping the MEA down with, e.g. a smooth Teflon piece. The cell was completed by forming the cathode current collector. A piece of backing identical with the anode one was lined up on the anode backing-MEA, whereupon a gold-plated stainless steel grid was laid. The whole sandwich was finally clamped together by the cathode current collector pressed against the Plexiglas support by two screws and bolts (Fig. 1B). Pure and dry hydrogen was used at the anode while the cathode was in contact with still air atmosphere. The gas pressures on both sides were at equilibrium with the room atmosphere. The hydrogen flow was controlled by a mass flowmeter (Brooks Instruments). The H_2 flow rate was 25 mL min^{-1} for all results presented herein, except for the results of Fig. 5, where the flow was varied. Save for the control of the hydrogen flow, the cell worked in complete passive mode. All reported measurements were recorded with the cell being horizontal and the cathode on top. For cell A1, the experiments were made with an EG&G potentiostat 273A. For one polarization curve (Fig. 3), the *iR*-drop was measured by current interrupts at each voltage as described by us in Ref. [15]. For cells A2, B2 and C2, a Zahner potentiostat was used. For these cells, the ohmic resistance was measured under steady-state operation at a voltage of 0.5 V by electrochemical impedance spectroscopy (EIS) and reading the high-frequency intercept of the spectra with the real axis. The cell temperature was measured by a thermocouple placed below the copper foil forming the anode current collector.

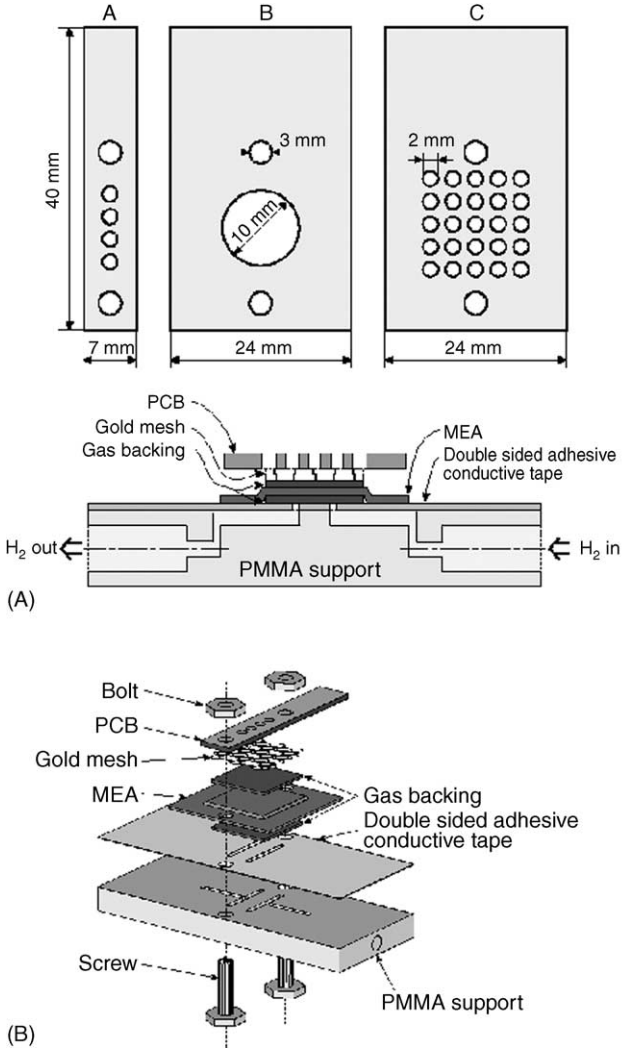

Fig. 1. (A) Top view of the three different geometries for the current collector of the cathode, defining the cells of types A, B and C and cross section of the cell. (B) Exploded view of the cell with the strip cathode current collector (type A).

3. Experimental results

3.1. Steady-state performance of cells with a strip cathode CC (type A)

Fig. 2 shows the cell voltage of cell A1 and its power density as a function of the current density. These curves demonstrate the good performance of this cell. A power density of 300 mW cm^{-2}, curve (b) was reached at a cell voltage of 0.5 V. Curve (a) was recorded shortly after cell installa-

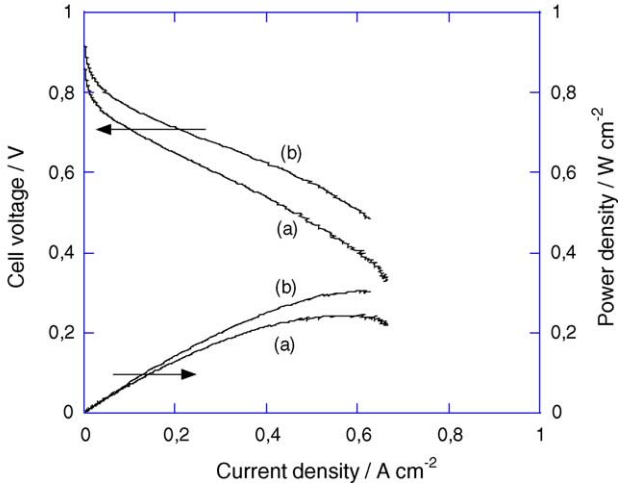

Fig. 2. Cell voltage and power density vs. current density of cell A1 (strip cathode CC). Curve (a) initial performance and curve (b) performance after 60 h at 0.5 V. No preconditioning prior to polarization. Sweep rate is 0.4 mV s^{-1}.

tion and is not as good as curve (b). Polarization curve (b) was recorded 3 h after the cell had been held for 60 h at the voltage of 0.5 V. The difference is most likely due to a drier MEA at inception. Not only the membrane conductivity but also the H_2 oxidation and O_2 reduction kinetics are known to be hampered by dry conditions. Polarization experiments repeated after curve (b) were alike. In this case, the enhancement from (a) to (b) was mainly due to an improvement in the oxygen reduction kinetics (increase from 0.4 to 3 mA cm^{-2} at 900 mV) while changes in ohmic losses were minor. Following, more information was obtained from the simultaneous measuring of the cell voltage and *iR*-drop. Fig. 3A shows as a function of the current density, the voltage of cell A1 (a), the *iR*-drop (b) and the cell voltage corrected for the *iR*-drop (c). Fig. 3B shows the corrected cell voltage as a function of the current density but in an *E* versus log *i* plane. From these two figures, it is deduced that: (i) the *iR*-drop was linear with current density, (ii) the *iR*-corrected curve displays a Tafel slope up to a current density of 0.2 A cm^{-2} (Fig. 3B) and (iii) at larger current density the deviation from the Tafel slope indicates the onset of combined control by kinetics and mass- and/or heat-transport at the cathode (for the last assertion it is assumed the hydrogen anode does not build up any sensible losses). Point (i) implies that the water content is uniform throughout the membrane and point (ii) means that the cathode is controlled solely by the kinetics of the oxygen reduction up to 0.2 A cm^{-2}. Next, the effect of the cell orientation on its performance was studied with the cell A2, a replicate of cell A1. The performance remained unaffected whether the MEA was horizontal (cathode either up or down) or vertical. The inconsequence of the cell orientation had already been observed by Schmitz et al. [12]. This input bodes well for a portable application of PEFCs. It is also a good piece of information for the building of models describing

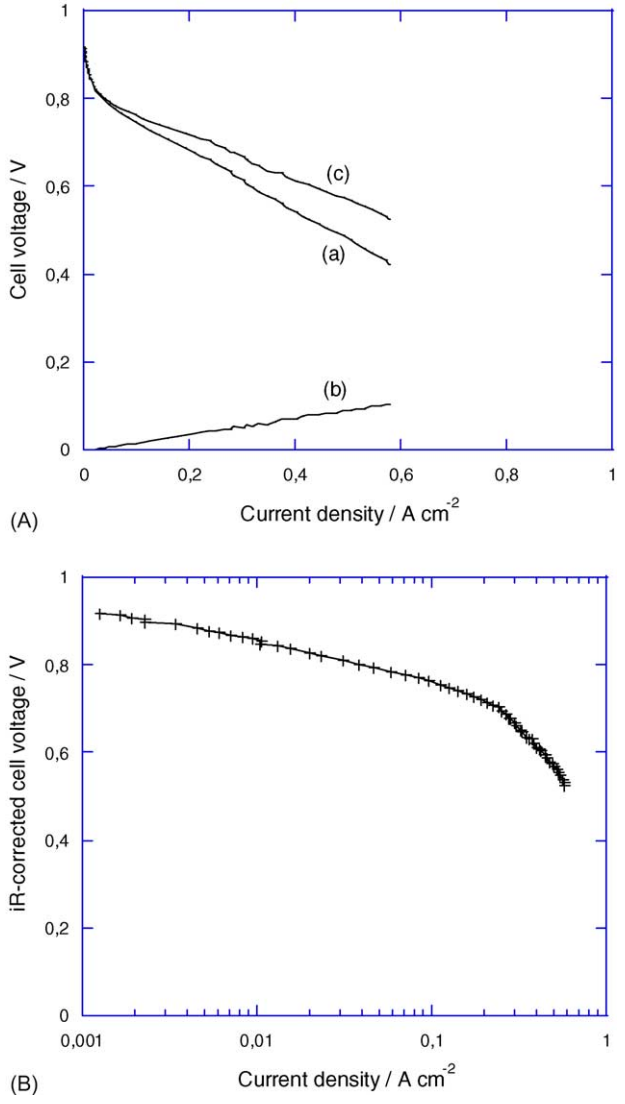

Fig. 3. (A) (a) Polarization curve of cell A1 (strip cathode CC) prior to 60 h test, (b) *iR*-drop measured with current interrupts, (c) *iR*-corrected curve. Sweep rate is 0.125 mV s^{-1}. (B) *iR*-Corrected polarization curve of cell A1 (strip cathode CC) in an *E*–log *i* plane.

coupled mass- and/or heat-transport in air-breathing PEFC cathodes.

A crucial aspect of passive fuel cells is their ability to dispose of the heat produced by the electrochemical reaction. Fig. 4 presents the cell temperature obtained on cell A3 (strip cathode CC) as a function of the produced heat per square centimeter of active area. The cell voltage was held constant for half an hour to reach a steady state, the temperature and current density were then measured. This was done in sequence from a cell voltage of 0.8 V down to 0.4 V and up again, by steps of 100 mV. The heat density was calculated according to the following equation: $q = i(1.21 - \Delta E)$, where i is the current density, ΔE the cell voltage and 1.21 is the thermodynamic voltage. It is seen in Fig. 4 that the increase in temperature is about linear with the heat density up to 0.6 W cm^{-2}. No hysteresis occurred when bringing the volt-

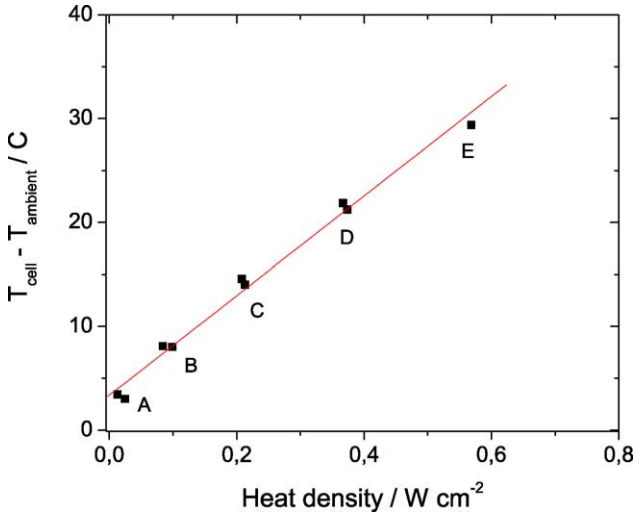

Fig. 4. Cell temperature–ambient temperature against heat density. Cell A3. Mean values: (A) 0.8 V, 31 mA cm^{-2} ; (B) 0.7 V, 179 mA cm^{-2} ; (C) 0.6 V, 345 mA cm^{-2} ; (D) 0.5 V, 521 mA cm^{-2} and (E) 0.4 V, 702 mA cm^{-2}.

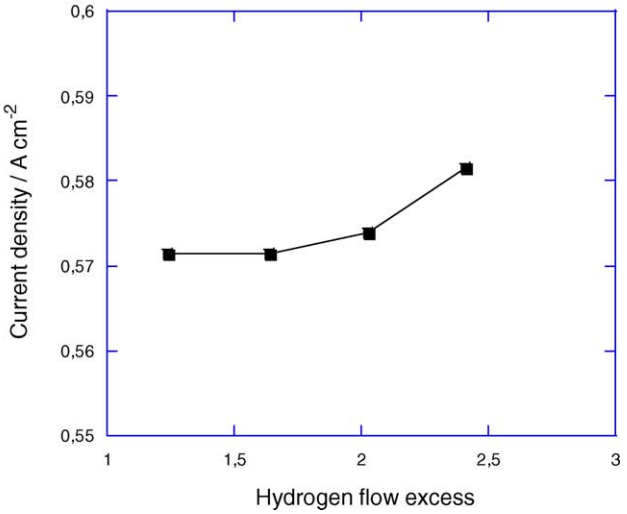

Fig. 5. Effect of the hydrogen flow. Current density of cell A2 (strip cathode CC) against the excess of hydrogen flow. Cell voltage is 0.5 V.

age up again (double points at 0.5, 0.6, 0.7 and 0.8 V). The linear fitting yields a heat exchange coefficient of 48 K W^{-1} cm^2 for this cell design, meaning the cell is heated up by 48 K if the heat production arising from the reaction is 1 W cm^{-2}. These values are based on the active surface area, about 2 cm^2. A rapid calculation shows that a water production corresponding to 1 A cm^{-2} has a cool-off power of 0.21 W cm^{-2}. With the present cell, this represents only 25–30% of the total heat production, independently of the working point (cell voltage or current density). Thus, most of the cooling occurs through the surface area between the cell elements and ambient air. Whether the electrochemically active area is the right area to consider for heat exchange is unclear. The cell dimension is about 12 cm^2 and some cooling must also occur at the interface between the copper film outside of the active area and air. In any case, Fig. 4 allows us to make a good estimation of the steady-state temperature of the cell at any point of its polarization curve: knowing the voltage and current density, the heat density is calculated and the temperature can be read by interpolation from Fig. 4.

Next, the effect of the hydrogen flow on the performance of such a cell was investigated. In practical applications, high fuel utilization is requested. Beside overall cell efficiency and hydrogen leakage through the membrane, a simpler source of less-than-unity utilization of the fuel is the average excess of fuel passed through the anode(s). An overall excess ratio is defined as the fuel flow (mol s^{-1}) entering the anode(s) to the overall flow consumed by the cell(s) in the anodic reaction. Thus, if the excess ratio is unity the fuel is completely oxidized (dead-end mode) and if larger than unity, part of the fuel is not oxidized electrochemically. In this study, the variation of the hydrogen excess was made by holding the cell voltage at 0.5 V and varying the hydrogen flow. The overall current of the cell was measured, and from it, the volumetric flow of hydrogen that was oxidized could be computed according to Faraday's law and the law for perfect gases. For a total current I, the flow of oxidized hydrogen is $N = RTI/(2PF)$, where R is the gas constant, T the room temperature, I the current, P the atmospheric pressure and F is the Faraday's constant. This yields $N = 7.43$ mL min^{-1} of hydrogen for a current of 1 A. The cell active area is about 2 cm^2. Fig. 5 presents the current density of cell A2 as a function of the hydrogen excess. It is seen that a hydrogen excess ratio of 1.2 was sufficient to reach a performance very close to that obtained with our standard hydrogen flow of 25 mL min^{-1}. For the sake of comparison, the latter flow corresponds to an excess ratio of 2.8 at a current density of 0.6 A cm^{-2}.

3.2. Startup of cells with a strip cathode CC (type A)

Two different startup procedures were investigated. In first mode, the cell was let at open circuit potential for a long time prior to suddenly decreasing and holding its voltage at a constant value. In second mode, the cell was conditioned prior to applying the aforementioned procedure. The conditioning consisted of (i) holding the cell at 0.5 V for a time sufficient to reach a steady state and (ii) letting the cell at open circuit for 5–10 min so that it cooled down to 22 °C or less. Fig. 6A shows how the current density of cell A3 evolves with time during the first 30 min of a potentiostatic control at 0.5 V for the two-startup procedures. Both curves display a sharp increase of the current with time in the first 30–40 s. After only 1 s, the current densities were 0.11 and 0.37 A cm^{-2} for modes 1 and 2, respectively. In mode 1, the current reaches a maximum after 30 s and decreases sharply in the next 10 s to reach a pseudo-steady state. In mode 2, the peak of current density is at 40 s but broader and the current drops to a pseudo-steady state in the next 30 s. Fig. 6B presents the parallel variation of the cell temperature as a

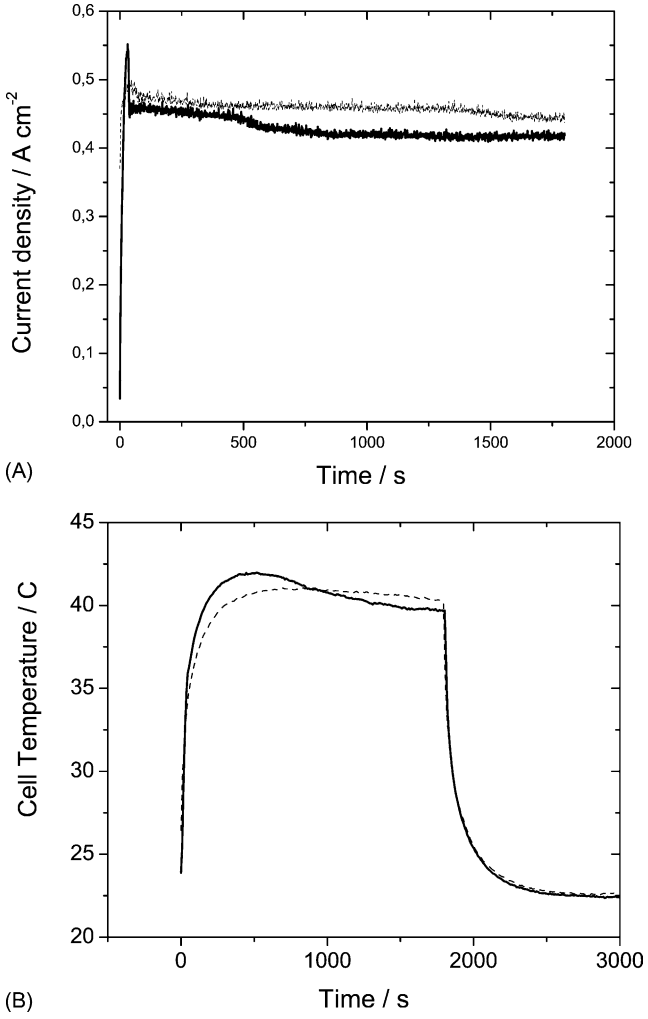

Fig. 6. Effect of the startup procedure. Response of cell A3 (strip cathode CC) to potential step from OCP to 0.5 V (t = 0 s) and back to OCP (t = 1800 s). Mode 1 means the cell was at rest for a long time prior to experiment and mode 2 means the cell was run at 0.5 V until steady state was reached and then rested for 5–10 min for cooling down prior to experiment. (A) Current density vs. time. Mode 1 (darker line), mode 2 (dashed bright line). (B) Cell temperature vs. time. Mode 1 (darker line), mode 2 (dashed bright line).

function of time. In mode 1, the temperature rises sharply and displays a broad peak with a maximum at about 500 s to decrease slowly afterwards. In mode 2, there is no clear peak though the temperature reaches a maximum after 900 s and decreases smoothly afterwards. After open circuit (1800 s), the cell cools down the same way for both startup procedures.

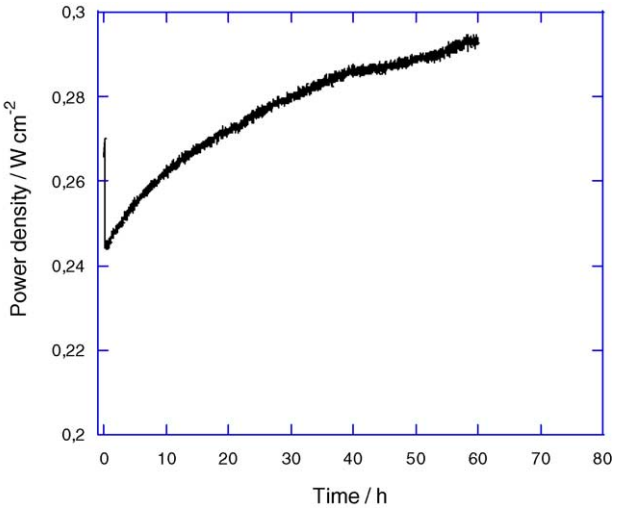

Fig. 7. Long-time test of cell A1 (strip cathode CC) at a voltage of 0.5 V. No cell preconditioning.

Extending the timescale of Fig. 6, Fig. 7 shows the behavior of cell A1 under a constant voltage of 0.5 V for 60 h. After a sharp drop during the first quarter hour, the cell performance steadily increased. The comparison of polarization curves recorded prior to and past the 60 h test (Fig. 2) tells us that the improvement was almost entirely due to catalytic activation of Pt. What is also by default demonstrated in Fig. 7 is that the MEA was not poisoned by copper in these specific conditions.

3.3. Geometry of the cathode CC and cell performance

With the very same cell house and MEA, three types of cathode CC were consecutively installed and tested. The cathode CCs were made of the same material but had different geometries (Fig. 1A). Table 1 shows values of the ohmic resistance of each cell. With air-breathing fuel cells, care must be taken when comparing ohmic resistances because they may depend on whether the cell was operated shortly before the measurement or not, and at what current density. However, with the thin membrane used in this study, the ohmic resistance seemed to be current-independent as suggested in Fig. 3A by the linear increase of the *iR*-drop with current density. Cell A1 seems to have a larger resistance than all other cells. Its resistance was measured prior to long-term testing. Possibly, the resistance of cell A1 had slightly de-

Table 1
Ohmic resistance of the cells as a function of the geometry of the cathode current collector

Cell	Cathode current collector	Ratio of open:active area at cathode	Ohmic resistance[a] (mΩ cm^2)	Peak power density (mW cm^{-2})
A1	Strip with holes	0.56	170[a]	305 at 509 mV
A2	Strip with holes	0.56	122[b]	287 at 485 mV
B2	Square with single hole	0.40	94[b]	250 at 495 mV
C2	Square with hole array	0.40	96[b]	287 at 490 mV

NB: these ohmic resistances are values averaged over the active area of the cell, i.e. about 2 cm^2.
[a] Extracted from *iR*-values measured by current-interrupt (Fig. 3A).
[b] Measured with EIS at a cell voltage of 0.5 V.

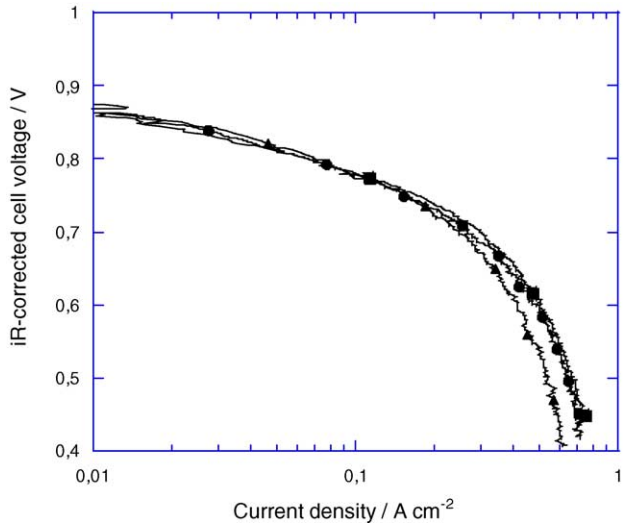

Fig. 8. Effect of the geometry of the cathode current collector. *iR*-Corrected polarization curves of cells A2-strip cathode CC (■), B2-single hole (▲) and C2-hole array (●). Sweep rate is 2 mV s^{-1}.

creased after its long-time testing, but not by much. Since the membrane type was the same for all cells, significant differences in the resistances of Table 1 must be sought at interfaces between components, e.g. between copper and backings. The copper PCB of cells A2, B2 and C2 had been polished prior to mounting and this may have enhanced their contact with the cathode backing. Another possibility is that the clamping pressure exerted by the screws was smaller for cell A1 than for the other cells. The comparison is easier between the cells A2, B2 and C2 because the cell house was identical and because the cells were preconditioned in the same way prior to measurement of the ohmic resistance. Cell A2 had an ohmic resistance larger than cells B2 and C2. This is in line with the larger fraction of open area for the cathode CC of cell A2. A larger open area means a smaller surface for the contact copper–carbon backing. In any case, the reported ohmic resistances are very satisfactory for air-breathing fuel cells. The resistance of the same membrane under fully humidified conditions is about 80 mΩ cm^2 or less. Thus, the remainder above 80 mΩ cm^2 in the present cells probably represents contact resistances.

Next, we present the polarization curves of the cells with various geometries for the cathode CC (cells A2, B2 and C2). Fig. 8 shows the *iR*-corrected polarization curves in a semi-logarithmic plot. The *iR*-correction was made assuming that the resistance found at 0.5 V by EIS (Table 1) is valid for all currents. First, it is clear from Fig. 8 that the various cells have a similar kinetics. Next, the curves depart from the Tafel behavior at current densities beyond about 0.2 A cm^{-2}, indicating thereby that the cathodes are then limited by mass- and/or heat-transport on top of the cathode kinetics. The three cells have close characteristics even in the mass- and/or heat-transport region with cells A2 and C2 (strip and hole array) being slightly better than cell B2 (single hole). Cell A2 (strip) has a larger ratio of open to close area (0.56), while cells B2 and C2 have an equal ratio of open to covered area (0.4). It was visually observed that the single hole had the tendency to be partly or completely obstructed by water droplets, especially during the long-term test. The peak power densities of the polarization curves of Fig. 8 are shown in Table 1. Differences in ohmic resistance among the cells A2, B2 and C2 are not decisive for their ranking in power density (Table 1). It is the heat and oxygen transport characteristics of a cell that sets its ranking.

4. Discussion

4.1. Specificities of the present design

(i) The exerted clamping pressure only helps to have a good electrical contact between the various components. In no means does it help in tightening the hydrogen compartment from the air. The latter is secured by the adhesion of the membrane onto the conductive adhesive layer lying on top of the anode CC. In a scaled-up process and for a single cell, the adhesive at this position needs not be conductive. Only the adhesive layer lying between the anode CC and the anode backing needs to be electron conductive. The fact that neither a mask nor a compression force is required for the tightening of the H_2 compartment simplifies the design and will help to reduce the distance between two consecutive cells serially connected on a board.

(ii) The membrane used in this study had active electrodes on the whole surface but the active area defined by the backings was much smaller than that. It is self-evident that in a scaled-up process MEAs would be customized and platinum deposited only onto the central active area.

(iii) Having the active electrodes on the whole MEA, the cathode active layer was electronically separated from the anode layer only by the edge of the polymer membrane, 20–30 μm thick. Any metallic dust or alike can thus create a local shortcut. This is believed to be instantly self-cutoff owing to the intense heat that would then be generated. No short circuits seemed to occur and high open circuit voltages were recorded.

(iv) Hydrogen gas was forced to flow through the anode backing. Permeability values of gas backings are sufficient to pass the required gas flows along distances of several centimeters with negligible pressure drop. In a board containing several such cells serially connected, the active areas would preferably be bands with a width of 2–5 cm and the fuel and electron flows would be organized in the width direction. The length of the active area would then only be limited by the size of the device that is to be powered. For example, 10 cells having each an active area of 2 cm × 10 cm and yielding at 0.5 V, a power density of 0.25 W cm^{-2} would give 50 W and 5 V.

4.2. Status of cell performance and insights on developments

In general, the cells had reproducible characteristics and were easily mounted. Looking at the polarization curve of Fig. 3, at a cell voltage of 0.5 V the losses (about 700 mV) can be divided into 71% losses stemming from the oxygen reduction kinetics (obtained by extrapolating the Tafel slope), 17% from heat- and mass-transport presumably occurring at the cathode (difference between the extrapolated Tafel slope and the *iR*-corrected curve), and 12% from ohmic losses (obtained from current interrupts). These data give an overview of the situation. It is difficult to reduce the kinetic losses unless the platinum loading at the cathode is raised by much. Even so, for the kinetic gain to be effective at high currents, the heat- and mass-transport characteristics of the cathode must be simultaneously improved. For the latter, practical and modeling work of the water and heat management of such cells remains to be done. The figure of 17% loss given above skews indeed the importance of mass- and heat-transport losses at the cathode. For example, if the Tafel slope were extended up to a current density of 1 A cm^{-2} in Fig. 3B, the cell voltage at that current density would become 0.5 V and the power density would reach 0.5 W cm^{-2}. When it comes to ohmic resistances, the ones reported in this study are low and can only little be decreased further. The lowest measured resistance in the present study was 94 mΩ cm^{-2} and would represent less than 7% of loss in the above calculation. In all, the performances of the air-breathing cells in this study top to about 40% of the peak power of the same MEA under controlled conditions.

Few studies have reported results of PEFC cells working in an air-breathing mode. Schmitz et al. [12] using PCB technology obtained a peak power of 100 mW cm^{-2} at 0.5 V for a single cell of 10 cm^2. The cathode was air-breathing, the anode fed with pure hydrogen and the MEA was Primea 5510 from Gore. Since the materials used in Ref. [12] and in the present study are almost the same, the difference in performance must be due to the cell design. Possibly, the heat removal of the present design is more effective because the cell is smaller, with faster natural convection at the sides of the active area than in the center. In Fig. 8 of Ref. [12], one can read an anode temperature of 50 °C at a current density of 0.25 A cm^{-2}. At the same current density, the cell of this study had a temperature of about 32 °C. Meyers and Maynard [10] using a silicon wafer reported a peak power of 60 mW cm^{-2} with forced flows of H_2 and O_2. Yu et al. [8] reported a peak performance of 200 mW cm^{-2} with pure H_2 and O_2 and forced flows. The active area was 10 cm^2 and the Pt loading 0.4 mg cm^{-2} per electrode. The ohmic resistance was no less than 0.7 Ω cm^{-2}. Finally, O'Hayre et al. [13] have published results using PCB technology. A peak performance of 550 mW cm^{-2} (and even 700 mW cm^{-2} for a clamped cell) was reached with pure O_2 and pure H_2 but dropped to 200 mW cm^{-2} when switching to air and H_2. Moreover, the reactant flows were controlled and the cathode was not air-breathing. The Pt loading was 2 mg cm^{-2}.

From the present and previous studies made by others, it does not seem that silicon technology gives better results and it is more complex and expensive than the PCB technology [12–14]. Next, copper is but one possibility among other materials. It was used because of the immediate availability of copper foils with a conductive adhesive layer. The bulk resistance of the material chosen for the CC of a planar PEFC should preferably lie in the range of 10^{-8}–10^{-7} Ω m. Let us imagine a serial connection of cells with the active area being 2 cm wide in the direction of the current and with a cell interdistance of 1 cm. Then, the repeating unit (a cell) is 3 cm wide. If the current density is 1 A cm^{-2}, the bulk resistance of the CCs is 10^{-7} Ω m and their thickness 100 μm, it can be calculated that the ohmic losses in the bulk of the CCs would be 6 mV per cell at that current density. Aluminum, copper and silver have bulk resistivities in the range of 1.5×10^{-8} to 2.5×10^{-8} Ω m. Numerous alloys would qualify too, e.g. Cu–Ni (10%) or Fe–Ni (1%) have bulk resistivities of about 10^{-7} Ω m. The next question is the inertness of such materials or alloys in the PEFC environment. Even though these materials are not supposed to be in direct contact with the acidic polymer present in the MEA, the environment is wet and corrosive, especially at the hydrogen side, where oxide layers are unstable. The problem can be circumvented by plating a bulk material of high conductivity with a thin layer of a noble metal (e.g. gold) or of a metal that passivate in this environment, e.g. Cr and Ni as was investigated by Schmitz et al. [14].

5. Conclusions

Single PEFCs were fabricated and yielded a peak power density of 300 mW cm^{-2} in an air-breathing mode and with pure H_2. The Pt loading was 0.3 mg cm^{-2} and the cell area 2 cm^2. The main specificities of the design are:

(i) As anode CC, a copper foil with a layer being both adhesive and conductive. That layer tightened the H_2 compartment without mask or clamping pressure and secured a good electronic contact with the anode backing.
(ii) A three-layer air-breathing cathode comprising a backing, a stainless steel net and a PCB cathode CC with a ratio of open:close area of 40% or more.

The ohmic resistance of the cells was in the range of 95–170 mΩ cm^{-2}. In operation at peak performance, 71% of the losses stemmed from the slow O_2 reduction, 17% or more from slow mass- and/or heat-transport at the cathode, and 12% or less from ohmic losses occurring mainly in the membrane. The onset of mass- and heat-transports at the cathode occurred at a current density of about 0.3 A cm^{-2} and it is the most critical feature to understand and optimize in order to reach better performances.

References

[1] C.K. Dyer, J. Power Sources 106 (2002) 31.
[2] S.C. Kelley, G.A. Deluga, W.H. Smyrl, AIChE J. 48 (2002) 1071.
[3] A. Heinzel, R. Nolte, K. Ledjeff-Hey, M. Zedda, Electrochim. Acta 43 (1998) 3817.
[4] A. Heinzel, C. Hebling, M. Müller, M. Zedda, C. Müller, J. Power Sources 105 (2002) 250.
[5] S.J. Lee, A. Chang-Chien, S.W. Cha, R. O'Hayre, Y.I. Park, Y. Saito, F.B. Prinz, J. Power Sources 112 (2002) 410.
[6] H.A. Gasteiger, J.E. Panels, S.G. Yan, J. Power Sources 127 (2004) 162.
[7] J. Yu, P. Cheng, Z. Ma, B. Yi, Elecrochim. Acta 48 (2003) 1537.
[8] J. Yu, P. Cheng, Z. Ma, B. Yi, J. Power Sources 124 (2003) 40.
[9] G. D'arrigo, S. Coffa, R.C. Spinella, European Patent EP1,258,937 (2002).
[10] J.P. Meyers, H.L. Maynard, J. Power Sources 109 (2002) 76.
[11] H.L. Maynard, J.P. Meyers, US Patent 6,541,149 (2003).
[12] A. Schmitz, M. Tranitz, S. Wagner, R. Hahn, C. Hebling, J. Power Sources 118 (2003) 162.
[13] R. O'Hayre, D. Braithwaite, W. Hermann, S.-J. Lee, T. Fabian, S.-W. Cha, Y. Saito, F.B. Prinz, J. Power Sources 124 (2003) 459.
[14] A. Schmitz, S. Wagner, R. Hahn, H. Uzun, C. Hebling, J. Power Sources 127 (2004) 197.
[15] J. Ihonen, F. Jaouen, G. Lindbergh, A. Lundblad, G. Sundholm, J. Electrochem. Soc. 149 (2002) 448.